

Contents lists available at ScienceDirect

Applied Geochemistry

journal homepage: www.elsevier.com/locate/apgeochem



Reactivity of binary manganese oxide mixtures towards arsenite removal: Evidence of synergistic effects

Boyoung Song ^a, Elizabeth B. Cerkez ^b, David E. Grandstaff ^a, Christopher M. Goodwin ^c, Thomas P. Beebe Jr. ^c, Bojeong Kim ^a, ^{*}

- ^a Department of Earth and Environmental Science, Temple University, Philadelphia, PA, 19122, USA
- ^b Department of Chemistry, Temple University, Philadelphia, PA, 19122, USA
- ^c Department of Chemistry and Biochemistry, University of Delaware, Newark, DE, 19716, USA

ARTICLE INFO

Editorial handling by Dr. Z Zimeng Wang

Keywords:
Arsenic
Hausmannite
Manganite
Binary
QXAS
HRTEM
Aggregation structures

ABSTRACT

The effects of manganese (Mn) mineral mixtures on arsenite (As(III)) removal (i.e., the sum of As(III) oxidation to As(V) and As species adsorption) were systematically quantified for the first time using varying ratios of hausmannite and manganite, common Mn(III)-containing oxides that often exist as mixtures in natural environments. Due to smaller particle sizes and a higher surface area, hausmannite alone exhibited a total As(III) removal of 8.86 μ M m⁻² at pH 5, almost double that of manganite, 4.63 μ M m⁻², with initially fast but then subsequently slower As(III) oxidation and Mn(II) production rates. Both minerals showed a substantial decrease in As(III) removal as pH increased. High resolution transmission electron microscopy (HRTEM) analysis showed mineral edge sites initially and preferably consumed for As(III) oxidation. Mixtures of hausmannite and manganite resulted in enhanced As(III) removal (9.62–11.2 μ M m⁻²) relative to the single minerals at pH 5, increasing with increasing manganite quantities. The mineral mixtures also displayed two reaction phases, where As(III) oxidation and Mn(II) production were initially fast but then slowed after the first hour. Further, the mineral mixtures produced a Mn(II):As(V) ratio higher than the theoretical two, indicating enhanced mineral dissolution than that of a single Mn oxide. Enhanced reactivity was attributed to the aggregation structure of mixtures, as the presence of manganite effectively limited the aggregation of hausmannite particles, as observed in HRTEM, promoting the exposure of highly active edge sites for the surface-mediated reactions. Thus, mineral mixtures may serve as a better surrogate than a single mineral to examine the extent and magnitude of As(III) removal in natural environments, by more closely reflecting the heterogeneity and complexity in surface interactions and aggregation structures between the minerals.

1. Introduction

Manganese (Mn) is the third most abundant transition metal, and occurs in various (oxyhydr)oxide forms (hereafter, Mn oxides) in the Earth's crust (Post, 1999). Mn oxides possess large specific surface areas, structural variants (e.g., impurities, defects, and vacancy sites), and multiple oxidation states (Mn(II/III/IV)) within the minerals, as well as an ability to achieve facile interconversions between these different Mn oxidation states (Elzinga, 2011; Ilton et al., 2016; Luo et al., 2018; Peña et al., 2007; Post, 1992, 1999). These unique characteristics make Mn oxides highly reactive towards a wide range of inorganic and organic contaminants (Atique Ullah et al., 2017; Eitel et al., 2018; Hu et al., 2016; Shaughnessy et al., 2003; Taujale et al., 2016; Taujale and Zhang,

2012; Wilk et al., 2005; Yin et al, 2011, 2014; Zhang et al., 2015) and thus they are considered to be influential sorbents and strong oxidants in the environment (Fischel et al., 2015; Lefkowitz and Elzinga, 2015; Nicholson and Eley, 2007; Peacock, 2009; Post, 1999; Simanova et al., 2015; Simanova and Pena, 2015; Taylor and McKenzie, 1966; Villalobos, 2015; Ying et al., 2012).

Arsenic (As) is one of the most frequently studied environmental contaminants, and its concentration in drinking water is enforced at 10 μg per liter (10 μg L $^{-1}$) by the US Environmental Protection Agency (US EPA) and the World Health Organization (WHO) due to its adverse health effects. A large body of research has demonstrated that Mn oxides effectively oxidize more toxic arsenite (As(III)) to the less toxic arsenate (As(V)) (Barreto et al., 2020; Chiu and Hering, 2000; Fischel et al., 2015;

E-mail address: bkim@temple.edu (B. Kim).

^{*} Corresponding author.

Lafferty et al., 2010a; Manning et al., 2002; Mock et al., 2019; Parikh et al., 2010; Shumlas et al., 2016; Silva et al., 2013; Song et al., 2020; Wu et al., 2018), although the extent of the oxidative and subsequent adsorptive reactions of As with Mn oxides varies by mineral structure (Fischel et al., 2015), structural impurity (Song et al., 2020), pH (Barreto et al., 2020; Lafferty et al., 2010a; Parikh et al., 2008; Shumlas et al., 2016; Silva et al., 2013; Wu et al., 2018), as well as the presence of competing ions (Chiu and Hering, 2000; Lafferty et al., 2011; Mock et al., 2019; Parikh et al., 2010; Wu et al., 2018). In general, these research efforts have employed single mineral systems to evaluate the reactivity of Mn oxides towards As. However, single mineral systems may not closely reflect natural settings, considering that mixed Mn oxide phases are exceedingly common (Post, 1992, 1999; Taujale et al., 2016; Taujale and Zhang, 2012; Zhang et al., 2015) and phase transformations in Mn mineralogy readily occur by mild environmental changes (Elzinga, 2011; Hem and Lind, 1994; Lind, 1988; Luo et al., 2018; Ramstedt and Sjöberg, 2005). Thus, to more accurately understand how As interacts with Mn oxides in the environment, and to better inform potential remediation strategies, analyzing mixed mineral systems with As(III) is required.

While limited, there has been growing scientific and industrial interest in using mixed mineral phases for As removal in waterways. For instance, goethite (\alpha-FeOOH) and birnessite (MnO2) were used in a Donnan reactor to examine the relative extent and magnitude of As adsorption and As(III) oxidation between the two mineral phases, as a representative binary system of natural environments (Ying et al., 2012). Further, the superior efficacy of natural oxide samples that contained mixtures of birnessite, goethite, and hematite (Fe2O3) in As removal from discharge in landfill sites has been demonstrated (Deschamps et al., 2005). Alternatively, synthetic Fe-Mn binary oxides (FeMnOx) have also shown to be effective in As removal from wastewater streams (Zhang et al., 2007; Zhou et al., 2020). In addition, the single and binary oxides of magnetite (Fe₃O₄) and hausmannite (Mn₃O₄) were examined for their ability to remove As; where the highest As removal was recorded with the Fe-Mn binary nanomaterials composed of 50% Fe and 50% Mn (Garcia et al., 2014). Yet, no study has evaluated the reactivity of mixed phases in the Mn oxide family towards As(III) removal.

In the present study we aim to address this critical knowledge gap by investigating a mixed mineral system of Mn oxides, namely hausmannite (Mn₃O₄) and manganite (γ-MnOOH), and quantifying the adsorptive and oxidative capacity first of the single Mn oxides (i.e., single system, hausmannite only and manganite only) and then of Mn oxide mixtures (i.e., binary system, both minerals with varying ratios) at two different pHs, using As(III) as a probe. Hausmannite and manganite are the most common Mn(III)-containing oxides and are often found as mixtures in natural settings, as they can readily undergo transformation processes by mild environmental changes (Elzinga, 2011; Lefkowitz et al., 2013; Lind, 1988; Lind and Hem, 1993; Luo et al., 2018; Peña et al., 2007). Both minerals have also shown to be effective at oxidizing As(III) to As (V) (Barreto et al., 2020; Chiu and Hering, 2000; Guo et al., 2015; Silva et al., 2013; Song et al., 2020). Thus, binary systems composed of hausmannite and manganite may address the complexity and heterogeneity present in both natural and engineered systems, adequately serving as a model to assess changes in the environmental reactivity of Mn oxide mixtures toward As.

Specifically, three mineral mixtures were created for the binary system to depict scenarios where the minerals were present in equal weight percent (wt.%) (e.g., Haus 50 wt% and Mang 50 wt%, hereafter HM11) or where one dominated (e.g., Haus 20 wt% and Mang 80 wt% (hereafter, HM14), or Haus 80 wt% and Mang 20 wt% (hereafter, HM 41)). Then, the As(III) removal (i.e., sum of As(V) produced and As adsorbed), Mn release, Mn(II):As(V) ratio, as well as the rate of As(V) or Mn(II) production, were measured and compared between the single and binary mineral phases. In order to determine As speciation on the mineral surfaces, X-ray photoelectron spectroscopy (XPS) and quick X-

ray absorption spectroscopy (QXAS) analyses were used. High resolution transmission electron microscopy (HRTEM) was also employed to (1) identify any changes in mineral morphology as a result of As(III) oxidation, (2) visually confirm the formation of other Mn oxide phases induced by As(III) oxidation, and finally (3) investigate the aggregation structure and morphology of mineral mixtures in the binary system. Thus, the results of this study provide mechanistic understanding of the reactivity of different mixed mineral systems toward As oxidation and adsorption and how they diverge from single mineral systems and hence, potentially aid our ability to better predict As removal processes in both natural and industrial settings.

2. Materials and methods

2.1. Materials

All chemical agents and reference materials for the present study were of analytical grade or better, including manganese acetate tetrahydrate (Mn(CH₃COO)₂·4H₂O, 99+%, Acros Organics), manganese chloride (MnCl₂·4H₂O, 99+%, Acros Organics), acetone (CH₃COOH, ≥ 99.5%, Thermo Fisher Chemicals), ethyl alcohol (C₂H₅OH, 200 proof, Pharmco-Aaper), potassium persulfate (K₂S₂O₈, ≥99%, Fisher Chemical), sodium (meta)arsenite (NaAsO₂, ≥90%, Aldrich Chemistry), sodium arsenate dibasic heptahydrate (Na₂HAsO₄, ≥98%, Sigma Life Science), sodium chloride (NaCl, ≥ 99%, crystalline, Fisher Scientific), nitric acid (HNO₃, 67–70% (w/w), trace metal grade, Fisher Chemical), hydrochloric acid (HCl, 36.5-38% (w/w), Fisher Chemical), and sodium hydroxide (NaOH, ≥ 97.0%, pellet, Fisher Chemical). In addition, Mn and As standard solutions for the inductively coupled plasma-optical emission spectroscopy (ICP-OES) were sourced from J.T. Baker® (1000 μ g/mL (\pm 0.10% w/v) in HNO₃ (<3% w/w)), reagent grade for trace metal analysis) and TraceCERT® (1000 mg/L (± 2 mg/L) in HNO₃ (2% w/w)), respectively.

2.2. Synthesis of hausmannite and manganite minerals for single and binary systems

Minerals of hausmannite (Song et al., 2012, Song et al., 2020) and manganite (Hu et al., 2008) were synthesized based on existing protocols, with some modifications. Briefly, hausmannite was prepared by dissolving 0.49 g of Mn(CH₃COO)₂·4H₂O in 5 mL of deionized (DI) water (Barnstead Nanopure, Thermo Fisher Scientific, 18.2 mΩ-cm water with 1–5 ppb total organic carbon) followed by addition of 15 mL of acetone in a pressure glass flask. The solution was stirred vigorously and placed into a silicon bath at 60 °C for 8 h. After 8 h, the particles were collected, washed thoroughly with DI water and ethyl alcohol several times, and dried in an oven at 60 °C overnight. Manganite was prepared by adding 250 mL of 20 mM Mn(CH₃COO)₂·4H₂O in a 500 mL Pyrex bottle with 6.5 mM of K₂S₂O₈, and incubating the mixture in a silicon bath at 120 °C for 12 h with stirring. After 12 h, the particles were collected, washed thoroughly with DI water, and dried overnight at room temperature. Mineral mixtures to generate the binary systems were prepared by combining freshly synthesized minerals before each use either for characterization or reaction. Three different wt.% fractions between hausmannite and manganite were selected and labeled as HM41, HM14, and HM11.

2.3. Characterization of single and binary systems

Freshly made hausmannite and manganite (herein referred to as Haus and Mang) were characterized for crystal structure, surface area (SA), size, morphology, and aggregation state before use. For the structure analysis, powder X-ray diffraction (PXRD) measurements were collected with a D8 Advance X-ray diffractometer (Bruker, USA) equipped with Ni-filtered, Cu Kα radiation and a high-speed energy-dispersive linear detector (LYNXEYE). Samples were placed on a zero-

Table 1Single Mn oxide systems: Solution data collected after an 8-h batch reaction with As(III) at pH 5 and 7.

Solution pH	Single syste	em	$[As]_{aq}^{a}(\mu M)$	$[As(V)]_{aq}^{a}$ (\(\mu M\))	$[As(V)]^{b}$ $(\mu M \cdot m^{-2})$	$[As]_{ad}$ c (μM)	As(III) removal $(\mu M \cdot m^{-2})$	$[Mn(II)]_{aq}^{a}$ (μM)
5	Haus		203 (±2)	194 (±10)	7.12	47.4	8.86	362 (±11)
	Mang		247 (±4)	$23.4 (\pm 0.9)$	4.11	2.99	4.63	$31.3 (\pm 3.0)$
7	Haus		174 (±3)	$12.2~(\pm 3.7)$	0.45	75.7	3.24	$21.2 (\pm 3.7)$
	Mang	261 (± 5)		7.02 (± 2.49)	1.23	N/A	1.23	$3.59 (\pm 0.42)$

^a The data sets ([As]_{aq}, produced [As(V)]_{aq}, and release [Mn(II)]_{aq}) that were used to plot graphs in Fig. S4 ([Me] (μ M) vs. time).

background sample holder and measured from 10 to 80° (2θ) at a step size of 0.01° /s. Mineral identification was made using the DIFFRAC.EVA software with the American Mineralogical Crystal Structure Database (AMCSD).

The SA of Haus, Mang, and HM11 was measured in triplicate using $N_2(g)$ adsorption and desorption isotherm by a Quantachrome Monosorb surface area analyzer and then calculated using Brunauer-Emmett-Teller (BET) equation. Calibration for the SA measurement was made by using the standard material of 1 \mbox{cm}^3 of air (C series, Pressure lok® analytical syringe, Valco Instruments Co. Inc). All SA of minerals are reported with average SA value and corresponding standard deviation in the unit of $m^2 \cdot g^{-1}$.

(HR)TEM analysis was performed to determine mineral size, morphology, and aggregation state with a JEOL JEM2100 TEM operated at 200 keV. TEM samples of Haus, Mang, and HM11 were prepared by depositing 20–50 μ L of the pre-sonicated mineral suspension onto a 400-mesh carbon-coated copper grid (Electron Microscopy Sciences, Hatfield, PA, USA) and allowed to air-dry at room temperature.

2.4. Batch experiments and solution analyses

Batch experiments of either the single or binary systems were carried out in a 200 mL beaker in oxic conditions at a particle loading of 0.2 g $\rm L^{-1}$ in 10 mM NaCl solution. The mineral suspensions were preequilibrated at pH 5 or 7 for an hour before a small aliquot of As(III) (from 50 mM NaAsO₂ stock solution) was spiked into the suspensions (Chiu and Hering, 2000; Manning et al., 2002; Shumlas et al., 2016; Song et al., 2020; Ying et al., 2012), resulting in a final concentration of 250 μ M As(III). The batch reactions were run for 8 h in duplicate with titration of HCl or NaOH, if needed, to maintain a targeted pH.

During the 8 h batch reaction a total of 11 aliquots (each aliquot about 600–700 μ L) were collected at selected times (0, 0.25, 0.5, 1, 2, 3, 4, 5, 6, 7, and 8 h) with a 1 mL syringe, and filtered with 0.22 μ m syringe filter (SVDG, Millipore). Filtered aliquots were then analyzed with an Ion Chromatography system (Dionex ICS-1000, Thermo Scientific) for As(V) concentration. Filtrates were also analyzed for total dissolved As and Mn concentrations by ICP-OES (iCAP 7400, Thermo Scientific, equipped with CetacTM ASX-520 Autosampler), after acidified with concentrated HNO₃.

2.5. Mineral solids analyses

For As speciation, XPS and QXAS analyses were performed on the As (III)-reacted Haus and Mang at pH 5, using NaAs(III)O $_2$ and Na $_2$ HAs(V)O $_4$ as reference materials. The As(III)-reacted minerals were collected after each batch experiment, washed with DI water, dried and stored in a plastic glove bag (Erlab 2200ANM, Erlab INC.) that was constantly purged with N $_2$ gas, prior to analysis.

The XPS analysis was conducted with a K-Alpha⁺ XPS (Thermo Fisher Scientific), and the spectra were processed using CasaXPS, version 2.3.18 (CASA Software Ltd., UK). Both samples and reference compounds were ground and deposited on carbon tape, while minimizing exposure to air prior to the measurement. All measurements had survey spectra gathered with a pass energy of 100 eV, and high-

resolution spectra gathered for all elements detected, or expected, at a pass energy of 20 eV. Due to well-known beam damage on As-containing samples (Smith et al., 2005), spectra were gathered with a short acquisition time and were repeated to ensure there was no change in the As peak shape during measurements. The collected spectra were processed with Shirley background subtraction by non-linear least squares using CasaXPS, where the fitting parameters, full-width half max, area, and the peak locations were allowed to vary within a given range. The spectra calibration was made by using adventitious carbon at 284.6 eV.

To avoid As oxidation during measurements (Cerkez et al., 2015; Smith et al., 2005), QXAS analysis was performed at beamline 7-BM of the National Synchrotron Light Source II (NSLS II), Brookhaven National Lab (BNL), Upton, New York. The As *K*-edge spectra were collected in fluorescence mode over the course of 5 min (each scan ~30 s) using a passivated implanted planar silicon (PIPS) detector after beamline calibration with Pt foil. The collected spectra were then background-corrected, normalized, and averaged with Athena (Ravel and Newville, 2005).

3. Results and discussion

3.1. Mineral identification and characterization

Freshly synthesized minerals of Haus and Mang were analyzed for crystal structure, SA, size, as well as morphology, prior to their use in a series of batch reactions. First, the PXRD patterns of Haus and Mang well-matched those of the reference materials, hausmannite (AMCSD 0002024) and manganite (AMCSD 0010565), respectively, indicating that no other Mn mineral phases were present in the samples (See supporting information (SI) 1.1, Fig. S1). Secondly, the BET SA of Haus, Mang, and HM11 was measured to be 136 (\pm 1), 28.5 (\pm 0.4), and 88.4 (± 0.3) m²·g⁻¹, respectively, showing that Haus recorded the highest BET SA, whereas Mang the lowest. By using the BET SA and relative proportion of Haus and Mang in the binary systems, the SA of HM41, HM11, and HM14 was estimated to be 115, 82.4, and 50.0 $\text{m}^2\text{ g}^{-1}$, respectively. When comparing the BET SA and estimated SA of HM11 $(88.4 \text{ vs. } 82.4 \text{ m}^2 \text{ g}^{-1})$, less than 6% difference was observed between the values. Detailed calculation of SA for the binary systems is provided in SI 1.2 (Fig. S2 and Table S1). Finally, the results of TEM analyses indicated that the particle size and morphology of the two minerals also differ significantly. Specifically, Haus had an average particle size of 21.1 $(\pm 4.5) \times 16.7 \ (\pm 3.7)$ nm with pseudo-octahedral morphology (size analysis n = 516 nanoparticles across two different TEM grids) (Figs. S3 (a-d)). In contrast, Mang had an average dimension of 322 (± 158) \times 236 (± 110) nm with needle morphology (size analysis, n = 304 across two different TEM grids) (Fig. S3(e), (f)), which is similar to the size ranges reported by Ramstedt and Sjöberg (2005).

3.2. Single mineral systems

After the analysis and characterization, the single mineral systems, Haus only and Mang only, were systematically assessed for oxidative and adsorptive capacity toward dissolved As species at two pH conditions (pH 5 and 7). The total As(III) removal by Haus or Mang was

^b [As(V)], the SA-normalized [As(V)] production in μ M·m⁻², is derived by using the [As(V)]_{aq} measurements.

 $^{^{}c}$ [As]_{ad} is estimated by subtracting the measured [As]_{aq} from the initial As(III) concentration (250 μ M).

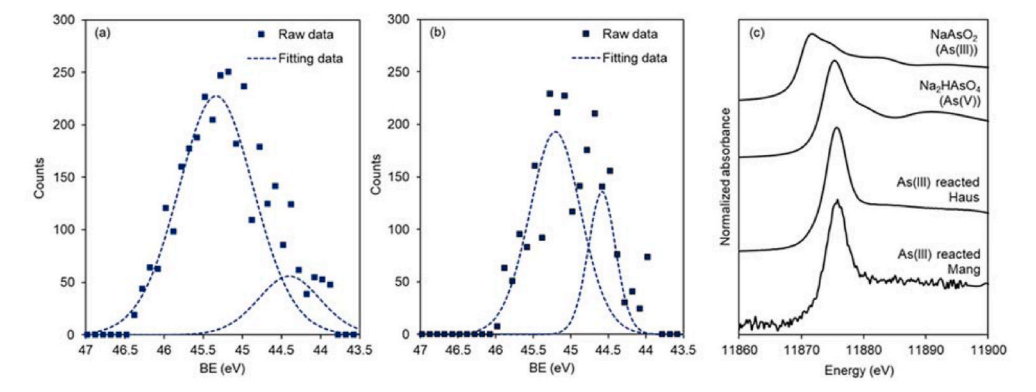


Fig. 1. XPS and QXAS analyses: XPS spectra of (a) As(III)-reacted Haus and (b) As(III)-reacted Mang samples at pH 5 (As $3d_{5/2}$ regions); (c) As K-edge XANES spectra of As(III)-reacted Haus and As(III)-reacted Haus and As(III)-reacted Mang (NaAsO₂ and Na₂HAsO₄ were used as reference compounds for As(III) and As(V), respectively).

estimated by summing As(V) measured in solution (i.e., $[As(V)]_{aq}$) and As species adsorbed onto the surface (i.e., $[As]_{ad}$). In addition, the release of Mn(II) and the stoichiometric ratio of Mn(II):As(V) by Haus or Mang were measured and compared.

3.2.1. Single mineral systems: As oxidation and adsorption

At pH 5, Haus oxidized approximately 78% of the initial As(III) to As (V), producing 194 μ M of [As(V)]_{aq} after 8 h of reaction (Table 1). In contrast, Mang oxidized only 9.4% of added As(III) to As(V), producing 23.4 μ M of [As(V)]_{aq}. Since Haus had a higher BET SA than Mang, when normalizing [As(V)]_{aq} by the mineral's SA, Haus and Mang produced 7.12 and 4.11 μ M m⁻², respectively. At pH 7, [As(V)]_{aq} was measured to be 12.2 and 7.02 μ M for Haus and Mang, respectively, indicating a significant decrease in As(V) production at higher pH. Similar to pH 5, Haus resulted in more [As(V)]_{aq} than Mang at pH 7, but after SA normalization of As(V) production Haus generated 0.45 μ M m⁻², whereas Mang 1.23 μ M m⁻², emphasizing that the oxidizing ability of Haus was more dependent on pH compared to Mang.

The extent of As adsorption (either As(III) or As(V)) onto the mineral surface was estimated by subtracting measured [As]_{aq} from the initial As concentration (250 μ M). At pH 5, less than 20% of the initial As was estimated to be adsorbed onto the surface of Haus, whereas at pH 7. more than 30% of initial As was adsorbed after 8 h. Thus, while the oxidative capacity of Haus decreased as pH increased, the mineral's adsorption ability increased with increasing solution pH. These findings indicate that at low pH the primary pathway of As removal in Haus was via As(III) oxidation, whereas at high pH As(III) adsorption was favored. In contrast, less than 2% of As adsorption occurred on Mang at both pHs, indicating that solution pH has little influence on the adsorption ability of Mang. Overall, total As(III) removal estimated by Haus and Mang was 8.86 and 4.63 $\mu M~m^{-2}$ at pH 5, and 3.24 and 1.23 $\mu M~m^{-2}$ at pH 7, respectively, implying that under all scenarios Haus in pH 5 solution was the most efficient for As(III) removal, whether by adsorption and/or oxidation to As(V). The detailed procedure for the estimation of As(III) removal is provided in SI section \$2.1.

The pH dependence of As(III) removal in the single mineral system can be attributed to changes in the surficial interactions between the As species and the mineral induced by solution pH. Arsenite $(H_3AsO_{3(aq)})$ is neutral at both pH conditions used, while arsenate is negatively charged, either $H_2AsO_4^-$ (aq) at pH 5 or $HAsO_4^2^-$ (aq) at pH 7 (Smedley and Kinniburgh, 2002). The point of zero charge (PZC) values of Haus and Mang are known to be below pH 5.0 (Song et al., 2020; Weaver and Hochella, 2003) and above pH 7.5 (Ramstedt et al., 2004), respectively. Hence, Haus has a neutral or slightly negative surface charge at pH 5, whereas, at pH 7, it is negatively charged. Therefore, the initial interaction of Haus with As(III) is electrostatically favorable at pH 5, but not at pH 7. As shown in the solution analysis, Haus is a weak sorbent for the As(V) species, since the negatively charged As(V) oxyanions are readily

released into solution once they are formed. On the other hand, Mang possesses a positive surface charge at both pHs, and hence, the adsorption of As(V) on the mineral surface is preferred. However, due to the lack of initial As(III) interaction on the positively-charged Mang surface, formation of As(V) is limited and therefore unreacted arsenite accounts for the majority of As in solution. Thus the solution pH plays a critical role in As oxidation and retention by single Mn(III) oxide systems.

3.2.2. Single mineral systems: post-reaction surface analysis

To confirm the As species on the mineral phases, XPS and QXAS analyses were performed on the mineral samples after reaction with As (III). Due to the very small amounts of As(V) detected by IC at pH 7, both surface analyses were only performed on Haus and Mang samples reacted with As(III) at pH 5. For XPS analysis, the As $3d_{5/2}$ peak was used to detect the presence and oxidation state of As on the mineral surface (Nesbitt et al., 1998; NIST X-ray Photoelectron Spectroscopy Database, 2000). Previous studies display As $3d_{5/2}$ binding energies for As(III) and As(V) located between 44.3-44.5 and 45.2-45.6 eV, respectively (Nesbitt et al., 1998; Ouvrard et al., 2005). Prior to exposure to As(III), no visible signal was observed in this As 3d region; however, upon As(III) introduction, a small As signal was observed in the single mineral systems. While low in intensity, peak fitting of the As(III)-reacted Haus showed peaks located at 45.3 and 44.4 eV, corresponding to 83% As(V) and 17% As(III), respectively (Fig. 1(a)). The As(III)-reacted Mang produced similar results, where peak fitting yielded 78% As(V) and 22% As(III) (Fig. 1(b)). The peak locations match well with previously reported values, indicating both arsenate and arsenite present at the mineral surface (Nesbitt et al., 1998; Ouvrard et al., 2005).

Furthermore, the positions of the As *K*-edge X-ray absorption near-edge structure (XANES) spectra of As(III)-reacted Haus and Mang matched that of the As(V) reference compound, located at ~11,875.0 eV (Fig. 1(c)). In total, the surface analysis agrees well with previous XPS and QXAS studies which noted that after As(III) adsorption/oxidation by Mn oxides, the As(V) moiety dominated on the mineral surfaces (Lafferty et al., 2010b; Manning et al., 2002; Shumlas et al., 2016; Song et al., 2020; Tournassat et al., 2002; Zhang et al., 2014).

3.2.3. Single mineral systems: mineral dissolution and morphology analysis

As a result of the As(III) oxidation by Haus and Mang, the concomitant production of Mn(II) was expected to occur in single mineral systems (Table 1). The theoretical stoichiometry results in a ratio of 2 to 1 of [Mn(II)] $_{aq}$ to [As(V)] $_{aq}$ for reductive dissolution, as shown in our prior study (Song et al., 2020). At pH 5, Haus produced a ratio of 1.9, close to the theoretical ratio, whereas at pH 7, a lower ratio of 1.7 was measured. This pH dependence on the stoichiometry relation between Mn(II) and As(III) was also noted with birnessite (Scott and Morgan, 1995). A similar decrease in ratio as a function of pH increase was also observed with Mang, although the ratio of Mn(II) to As(V) was lower overall,

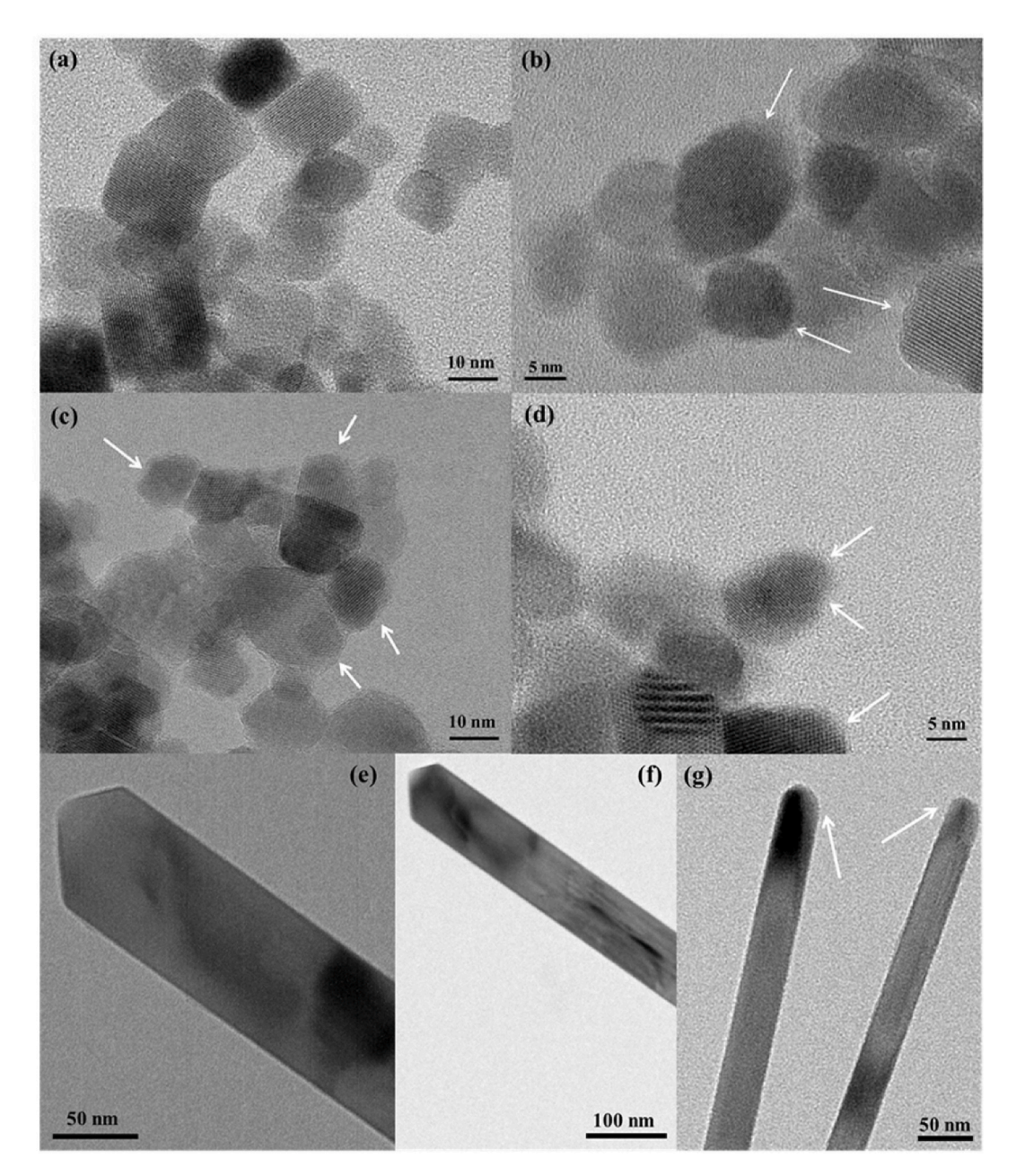
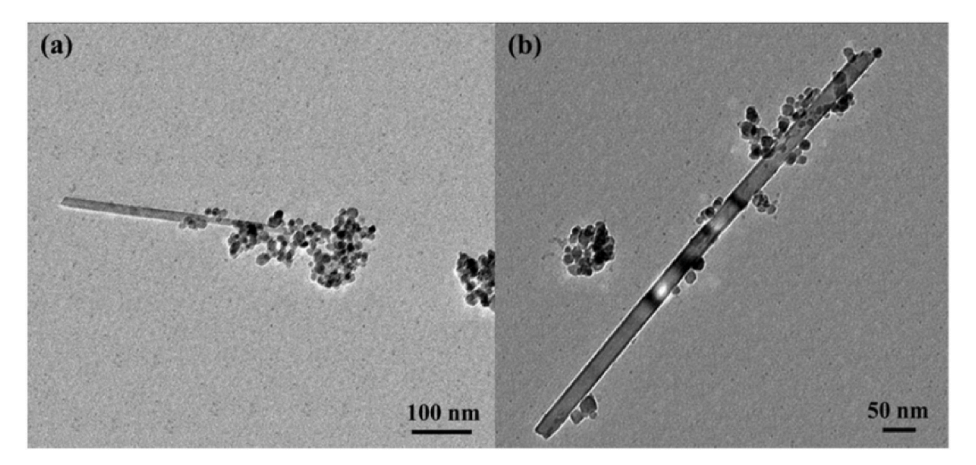


Fig. 2. (HR)TEM images of (a) pristine Haus; (b-d) As(III)-reacted Haus for 1 h; (e-f) pristine Mang; and (g) As(III)-reacted Mang after 8 h.



 $\textbf{Fig. 3.} \ \ \textbf{TEM images of newly-formed Mang in the As(III)-reacted Haus sample after 8 \ h.}$

Table 2
Binary Mn oxide systems: Solution data collected after 8 h with As(III) at pH 5.

Solution pH	Binary system	$[As]_{aq}^{a}(\mu M)$	$[As(V)]_{aq}^{a}$ (\(\mu M\))	[As(V)] ^b $(\mu M \cdot m^{-2})$	[As(V)] _{ad} ^c (µM)	As(III) removal $(\mu M \cdot m^{-2})$	$[Mn(II)]_{aq}^{a}$ (μ M)
5	HM41	247 (±1)	165 (±2)	7.17	2.61	7.30	$318 \ (\pm 16)$
	HM11	230 (±1)	138 (±4)	8.38	20.4	9.62	$296 \ (\pm 18)$
	HM14	241 (±1)	103 (±3)	10.3	8.70	11.2	$226 \ (\pm 13)$

- ^a The data sets ([As]_{aq}, produced [As(V)]_{aq}, and release [Mn(II)]_{aq}) that were used to plot graphs in Fig. S5 ([Me] (μ M) vs. time).
- ^b [As(V)], the SA-normalized [As(V)] production in μ M·m⁻², is derived by using the [As(V)]_{aq} measurements.

namely 1.3 and 0.4 for pH 5 and 7, respectively. The lower ratio exhibited by Mang may be ascribed to the potential stabilization of Mn (II) on the structure, as surface is primarily composed of unreactive basal planes, or to an enhanced rate of comproportionation reactions resulting in reformation of Mn(III), where either would result in a decreased concentration of Mn(II) in solution, thus lower the stoichiometric ratio (Jun and Martin, 2003).

As the mineral surface reacts with As(III), the mineral morphologies would be expected to be altered, both by consumption of reactive sites and transformation into more highly oxidized MnO₂ phases (Luo et al., 2018; Peña et al., 2007). Both Haus and Mang have faceted shapes (Fig. 2), with pseudo-octahedral (Fig. 2(a)) and needlelike morphologies (Fig. 2(e), (f)), respectively (more images in SI, Fig. S3), and these edges are most likely reactive and preferential sites for such surface reactions. The present study is the first to monitor changes in the mineral morphologies as Haus and Mang undergo reductive dissolution.

To visualize and emphasize such changes in the mineral morphology, HRTEM analysis was performed on Haus or Mang samples collected after 1 h or 8 h of reaction with As(III) at pH 5, respectively. HRTEM images of Haus exhibited spherical morphology (Fig. 2(b–d)) after the reaction. Lattice fringes of the particles were observed concurrently with rounded edges, suggesting that the edges of the Haus crystals are highly reactive and preferable for As(III) oxidation (target sites were marked with white arrows in the images).

In contrast, the needlelike Mang exhibited overall similar morphology to the unreacted one (Fig. 2(e), (f)) after the reaction, especially along the basal plane. The edges, however, became rounded after 8 h of reaction with As(III), similar to that of Haus (indicated by white arrows) (Fig. 2(g)). As seen in the images, Mang is dominated by the unreactive basal plane and reductive dissolution was only observed at the tips of the needles. Thus, this finding further supports the presence of more reactive sites in Haus and its close value to the theoretical Mn (II):As(V) ratio, as well as the lack of reactive sites in Mang and its deviation from the theoretical ratio.

In regards to mineral transformation, the formation of Mang was observed from the As(III)-reacted Haus sample after 8 h (Fig. 3). It is also noted that all Haus particles were comparably smaller and spherical, likely due to extensive dissolution as the reaction proceeded, suggesting the release of Mn occurs over the course of the reaction. In contrast, only Mang was detected in the Mang samples after 8 h reaction with As(III) (data not shown), indicating no transformation processes under these batch conditions.

3.3. Binary mineral systems

Observations of both the co-presence of Haus and Mang minerals in the same geological settings (Hem and Lind, 1994; Lind, 1988; Lind and Hem, 1993; Peña et al., 2007) and Mang formation during As(III) oxidation by Haus (Fig. 3) strongly suggest that a mixture of oxides should be analyzed to better understand As(III) interactions with Mn(III) oxides in real environments. To mimic varying quantities of the minerals, binary systems of Haus and Mang (HM41, HM11, and HM14) were assessed at pH 5, where enhanced reactivity had been observed in the single systems, for the total removal of As(III), the release of Mn(II), as

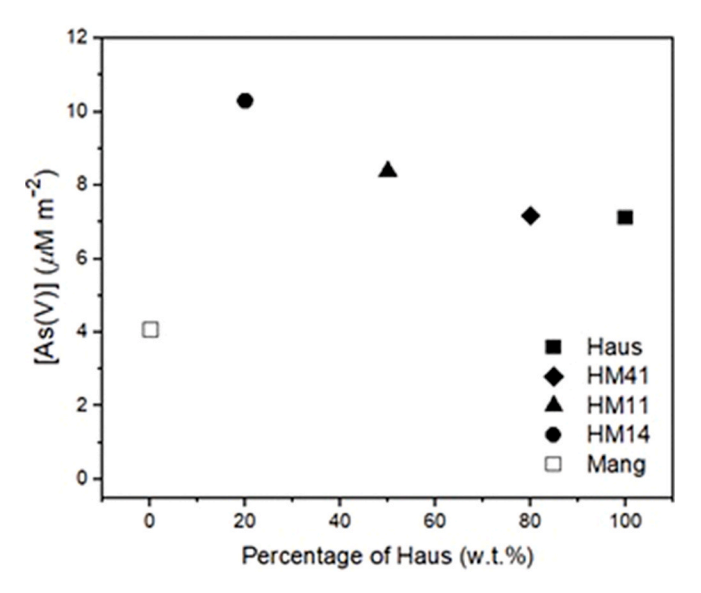


Fig. 4. Comparison of the SA-normalized [As(V)] production as a function of the percentage of Haus (wt.%) in the single and binary systems.

well as the stoichiometric ratio of Mn(II):As(V). The performance of binary mineral systems was compared to the single mineral systems to quantify potential cooperative reactivity of mineral mixtures, if present.

3.3.1. Binary mineral systems: As oxidation and adsorption

After 8 h of reaction with As(III), the mineral mixtures produced As (V)_{aq} in quantities relatively similar to Haus, but significantly higher than that of Mang (Table 2). The amount of As(V) produced in the binary systems increased as a function of increased ratio of Haus to Mang, where HM41 recording the highest [As(V)]_{aq}, 165 μ M, followed by HM11 and HM14, at 138 and 103 μ M, respectively. While a per massbased comparison shows increased As(V) with increased ratio of Haus, the mineral mixtures possess a varying SA by the relative wt.% fractions between Haus and Mang. When normalizing $[As(V)]_{aq}$ by the SA of mineral solids (Fig. S2 and Table S1) and comparing by this metric, the mixtures (HM41, HM11, and HM14) produced significantly more As(V) than the single minerals (Table 2). Notably, the As(V) per m² production increased as the percentage of Haus decreased (Fig. 4), which initially appears opposite to that of the single mineral system where, after SA normalization, Haus produced more As(V)_{aq} per m² than Mang (Table 1). This result indicates possible synergistic interactions between Haus and Mang that may be favorable to increase the overall reactivity toward As(III).

The quantity of As (either As(III) or As(V)) adsorbed on the mineral surfaces was found to be consistently low, less than 10% of initial As(III) throughout the reaction, leaving the majority of As species in solution, an observation similar to the single systems. Thus, when considering both As adsorption and oxidation, the binary mixtures recorded a total As(III) removal of 7.30, 9.62, and $11.2 \, \mu \text{M m}^{-2}$, for HM41, HM11, and HM14, respectively. The binary systems with higher Mang quantities (e.

^c [As]_{ad} is estimated by subtracting the measured [As]_{aq} from the initial As(III) concentration (250 μ M).

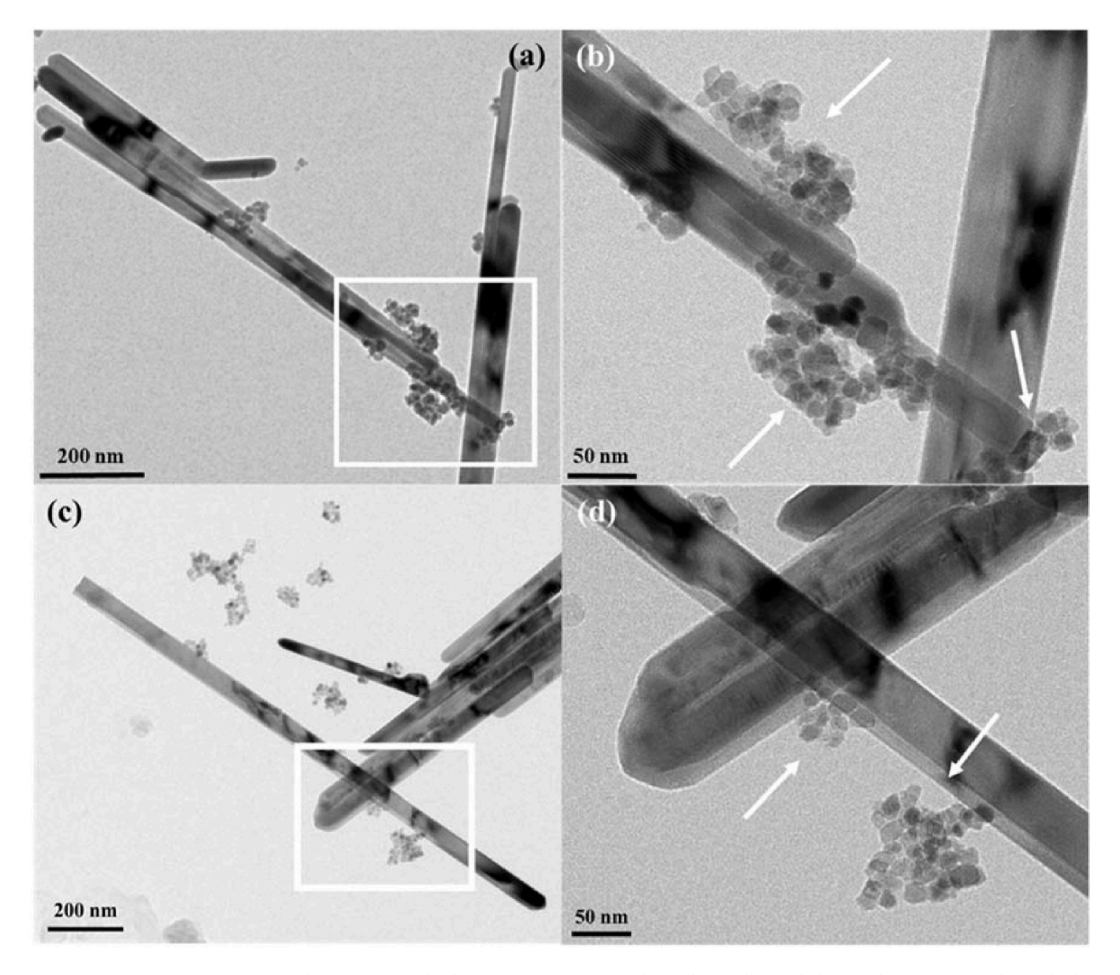


Fig. 5. TEM images of HM11 (50 wt% of Haus and of Mang in the binary system) (a) and (c) (left side) and their enlarged views (b) and (d) (white boxed area, right side).

g., HM 11 and HM14) showed a greater efficiency in As(III) removal than Haus. The total As(III) removal by the binary mineral systems is calculated in the same manner as the single systems, and detailed procedure is provided in SI section S3.1.

3.3.2. Binary mineral systems: mineral dissolution and aggregate structure analysis

The concomitant release of Mn(II) was also observed during the 8 h period in the binary systems. The $[Mn(II)]_{aq}$ in mineral mixtures resulted in Mn(II):As(V) ratios of 1.9, 2.1, and 2.2 for HM41, HM11, and HM14, respectively, showing when Haus was the dominant mineral phase (i.e., HM41), the Mn(II):As(V) ratio was close to the theoretical value of 2. As the Mang proportion increased in the mixtures, HM11 and HM14, the ratios increased. This result deviates from the single Mang system at pH 5, where the Mn(II):As(V) ratio of 1.3 was observed. The higher ratios noted in the binary systems could be attributed to an increase in the extent of mineral dissolution reactions, resulting from synergistic particle-particle interaction effects.

To better characterize the nature of surface interactions between Haus and Mang in the binary system, TEM analysis was performed on the mixtures. As noted above, the particle size and morphology of two minerals differ significantly, thus visual identification of one from the other is facile when they are present in mixtures (Fig. 3). Further, it was evident in the single systems that edge sites of Haus and Mang were reactive for As(III) oxidation and were preferably consumed in the initial phase of the reaction (Fig. 2(b-d), (g)).

Under the conditions (pH 5), Haus has a neutral or slightly negative surface charge, and hence, tends to form large aggregates. The presence of several large aggregates of Haus particles (size range: 230–490 nm)

was identified in TEM images (Figs. S3(a–c)). In contrast, Mang is positively charged at pH 5, and thus, remains dispersed as individual needles or forms stacks only a few needles thick, as shown in Fig. S3(e). Therefore, at pH 5 the surface interactions between two minerals are expected to be insignificant or limited due to weak electrostatic interactions. As seen in the TEM images of HM11, the two minerals do not form large aggregates (Fig. 5), instead small aggregates (size range: 70–160 nm) of Haus particles situated on the basal planes of Mang were observed. The presence of Mang thus appears to limit the formation of larger aggregates of Haus particles.

By forming small aggregates of Haus particles on the unreactive basal planes of Mang, more of the reactive edge sites of Haus become accessible for the As(III) oxidation reaction, without compromising the reactive surfaces of Mang. Therefore, these aggregate structures of the mineral mixtures may be favorable to increase the overall Mn oxides reactivity toward As(III). In a similar regard, the exposure of edge sites can also induce mineral dissolution by acidity (Jun and Martin, 2003; Luo et al., 2018; Peña et al., 2007; Song et al., 2020; Weaver et al., 2002), which may account for the higher Mn(II):As(V) ratios observed in the binary systems. Thus, these TEM observations provide visual evidences of the higher As(III) oxidation and removal efficiency, as well as the higher Mn(II):As(V) ratio noted in the binary mineral systems, especially HM11 and HM14, where the Mang fraction is greater. More TEM images of the aggregate structure of Haus and Mang are provided in SI (Fig. S6).

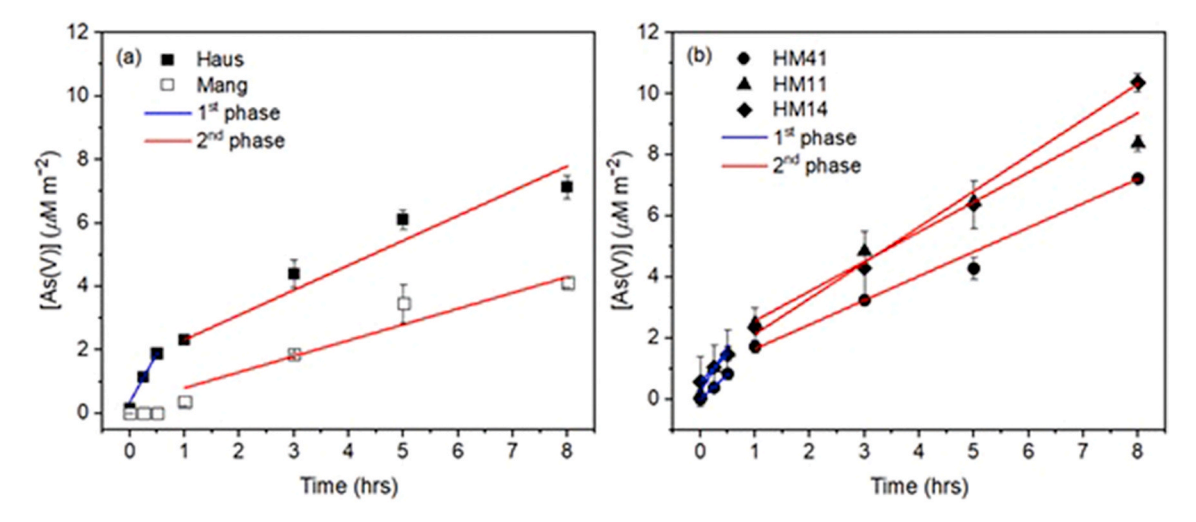


Fig. 6. Linear regression of the As(V) production over the course of the reaction by (a) Haus (square) and Mang (blank square) and (b) HM41 (circle), HM11 (triangle), and HM41 (diamond) after the mineral's SA normalization with the 1st (blue) and the 2nd (red) reaction phases. (For interpretation of the references to colour in this figure legend, the reader is referred to the Web version of this article.)

Table 3The calculated As(V) production rates from the single and binary systems and the linear regression lines shown in Fig. 6.

pH 5	System	1st phase		2nd phase		
		μM m ⁻² •h ⁻¹	R ²	μM m ⁻² ⋅h ⁻¹	R ²	
Single	Haus	3.49	0.99	0.68	0.94	
	Mang	N/A		0.54	0.93	
Binary	HM41	1.67	1.00	0.77	0.99	
	HM11	2.72	0.98	0.83	0.98	
	HM14	1.77	1.00	1.15	0.99	

3.4. Single and binary mineral systems: the As(V) and Mn(II) production rates

To further examine the synergistic effect observed in the binary system, a series of comparisons of As(V) and Mn(II) production rates of both the single and binary systems was performed by linear regression (Fig. 6 and Table 3). Due to the similarities in the results, only As(V) production rates were presented here, while discussion of the Mn(II) production rates were placed in the SI, section S3.3 (Fig. S7 and Table S2). From the SA-normalized As(V) production as a function of reaction time, the single Haus system resulted in two different rates (Fig. 6(a)), having an initial fast rate of 3.49 μ M m⁻² · h⁻¹ within the first hour, followed by a slower rate of 0.68 uM m⁻²·h⁻¹ through the rest of the reaction period (also with a slightly lower R² value) (Table 3). In contrast, the single Mang presented a rate of As(V) production, 0.54 μ M $m^{-2} \cdot h^{-1}$, which remained constant throughout the reaction (Fig. 6(a)). Overall, the rate analysis agrees well with HRTEM observations (Fig. 2), where after the exhaustion of preferred mineral edges for the reductive dissolution, the reaction rate slows, more significantly in the single Haus system than Mang, attributed to the larger quantity of reactive surface sites in Haus.

In the binary mineral system, all mixtures had similar initial rates of As(V) production, specifically 1.67, 2.72, and 1.77 μ M m⁻²·h⁻¹ for HM41, HM11, and HM14, respectively (Fig. 6(b) and Table 3). These initial rates were slower than that of the single Haus system but much higher than that of the single Mang system. Similar to the single systems, the As(V) production rates in the binary systems also decreased as the reactions proceeded, but the 2nd phase reaction rates of the binary systems were greater than that of the single Haus or Mang. The 2nd reaction phase rates of HM41, HM11, and HM14 were 0.77, 0.83, and 1.15 μ M m⁻²·h⁻¹ (Table 3), respectively (single Haus was 0.68 μ M

 $m^{-2} \cdot h^{-1}$), indicating that the presence of Mang enhanced the rate of As (V) production in the 2nd phase of the binary systems. This sustained reactivity observed in the binary system as a function of increased Mang loading is attributed to the dispersion of individual Haus crystals and the formation of smaller aggregates across the basal planes of Mang, exposing more reactive Haus surfaces, as previously noted in TEM analysis (Figs. 5 and S6). Such influence of particle aggregation on nanomineral dissolution reaction rates has been also shown elsewhere (Liu et al., 2009).

4. Conclusions

The present study systematically compared and contrasted single and binary Mn oxide systems for As(III) removal to better characterize the complexity and heterogeneity of natural environments, where single mineral phases of Mn oxides rarely exist, but mixed phases dominate. While the single Haus system was more effective at removing As(III). either by oxidation and/or adsorption, than Mang, in the binary mineral system the efficacy of As(III) removal increased as the Mang proportion in the system increased. HRTEM images, combined with rate measurements, provide insight into the preferential consumption of edge sites for As(III) oxidation, and when two minerals were present, aggregation structures of two minerals led to enhanced As(III) oxidation by exposing more reactive surfaces of Haus particles. Furthermore, these aggregate structures also accelerated the acidic dissolution of Haus, releasing more Mn(II) than the single Haus system, producing a higher Mn(II):As(V) ratio than the theoretical of 2. Thus, it is concluded that the presence of a Mn oxide can have additive or synergistic effects on the other Mn oxide's reactivity through modifying aggregation structures. The weaker electrostatic interaction between two minerals results in the greater overall performance in the surface-mediated redox reactions. The present study thus provides strong evidence that a mineral's reactivity in the environment can be significantly affected by the properties and relative quantity of a secondary mineral. Further works are planned to examine more combinations of Mn minerals found in natural settings for their environmental reactivity against the single mineral phase.

Declaration of competing interest

The authors declare that they have no known competing financial interests or personal relationships that could have appeared to influence the work reported in this paper.

Acknowledgments

This research was supported by the National Science Foundation under Grant No. 2003866. The authors acknowledge the support by the 7-BM beamline scientists, Syed Khalid and Steven Ehrlich, for QXAS data acquisition and analysis. The authors also acknowledge the use of 7-BM beamline of the National Synchrotron Light Source II, a U.S. Department of Energy (DOE) Office of Science User Facility operated for the DOE Office of Science by Brookhaven National Laboratory under Contract No. DE-SC0012704.

Appendix A. Supplementary data

Supplementary data to this article can be found online at https://doi.org/10.1016/j.apgeochem.2021.104939.

References

- Atique Ullah, A.K.M., Fazle Kibria, A.K.M., Akter, M., Khan, M.N.I., Tareq, A.R.M., Firoz, S.H., 2017. Oxidative degradation of methylene blue using Mn_3O_4 nanoparticles. Water Conserv. Sci. Eng. 1, 249–256. Barreto, M.S.C., Elzinga, E.J., Alleoni, L.R.F., 2020. Hausmannite as potential As(V)
- Barreto, M.S.C., Elzinga, E.J., Alleoni, L.R.F., 2020. Hausmannite as potential As(V) filter. Macroscopic and spectroscopic study of As(V) adsorption and desorption by citric acid. Environ. Pollut. 262, 114196.
- Cerkez, E.B., Bhandari, N., Reeder, R.J., Strongin, D.R., 2015. Coupled redox transformation of chromate and arsenite on ferrihydrite. Environ. Sci. Technol. 49, 2858–2866
- Chiu, V.Q., Hering, J.G., 2000. Arsenic adsorption and oxidation at manganite surfaces. 1. Method for simultaneous of determination of adsorbed and dissolved arsenic species. Environ. Sci. Technol. 2029–2034.
- Deschamps, E., Ciminelli, V.S.T., Höll, W.H., 2005. Removal of As(III) and As(V) from water using a natural Fe and Mn enriched sample. Water Res. 39, 5212–5220.
- Eitel, E.M., Zhao, S., Tang, Y., Taillefert, M., 2018. Effect of manganese oxide aging and structure transformation on the kinetics of thiol oxidation. Environ. Sci. Technol. 52, 13202–13211.
- Elzinga, E.J., 2011. Reductive transformation of birnessite by aqueous Mn(II). Environ. Sci. Technol. 45, 6366–6372.
- Fischel, M.H.H., Fischel, J.S., Lafferty, B.J., Sparks, D.L., 2015. The influence of environmental conditions on kinetics of arsenite oxidation by manganese-oxides. Geochem. Trans. 16, 1–10.
- Garcia, S., Sardar, S., Maldonado, S., Garcia, V., Tamez, C., Parsons, J.G., 2014. Study of As(III) and As(V) oxoanion adsorption onto single and mixed ferrite and hausmannite nanomaterials. Microchem. J. 117, 52–60.
- Guo, S., Sun, W., Yang, W., Li, Q., Shang, J.K., 2015. Superior As(III) removal performance of hydrous MnOOH nanorods from water. RSC Adv. 5, 53280–53288.
- Hem, J.D., Lind, C.J., 1994. Chemistry of manganese precipitation in Pinal Creek, Arizona, USA: a laboratory study. Geochem. Cosmochim. Acta 58, 1601–1613.
- Hu, C.C., Wu, Y.T., Change, K.H., 2008. Low-temperature hydrothermal synthesis of Mn₃O₄ and MnOOH single crystals: determinant influence of oxidants. Chem. Mater. 2890–2894.
- Hu, Z., Chen, D., Dong, J., Li, Q., Chen, Z., Yin, D., Zhao, B., Wu, C.M.L., Shek, C.H., 2016. Facile synthesis of hierarchical Mn₃O₄ superstructures and efficient catalytic performance. Phys. Chem. Chem. Phys. 18, 26602–26608.
- Ilton, E.S., Post, J.E., Heaney, P.J., Ling, F.T., Kerisit, S.N., 2016. XPS determination of Mn oxidation states in Mn (hydr)oxides. Appl. Surf. Sci. 366, 475–485.
- Jun, Y.S., Martin, S.T., 2003. Microscopic observations of reductive manganite dissolution under oxic conditions. Environ. Sci. Technol. 37, 2363–2370.
- Lafferty, B.J., Ginder-vogel, M., Sparks, D.L., 2010a. Arsenite oxidation by a poorly crystalline manganese-oxide 1. Stirred-flow experiments. Environ. Sci. Technol. 44, 8460–8466.
- Lafferty, B.J., Ginder-Vogel, M., Sparks, D.L., 2011. Arsenite oxidation by a poorlycrystalline manganese oxide. 3. Arsenic and manganese desorption. Environ. Sci. Technol. 45, 9218–9223.
- Lafferty, B.J., Ginder-vogel, M., Sparks, D.L., Zhu, M., Livi, K.J.T., 2010b. Arsenite oxidation by a poorly crystalline manganese oxides. 2. Results from X-ray absorption spectroscopy and X-ray diffraction. Environ. Sci. Technol. 44, 8467–8472.
- Lefkowitz, J.P., Elzinga, E.J., 2015. Impacts of aqueous Mn(II) on the sorption of Zn(II) by hexagonal birnessite. Environ. Sci. Technol. 49, 4886–4893.
- Lefkowitz, J.P., Rouff, A.A., Elzinga, E.J., 2013. Influence of pH on the reductive transformation of birnessite by aqueous Mn(II). Environ. Sci. Technol. 47, 10364–10371.
- Lind, C.J., 1988. Hausmannite (Mn_3O_4) conversion to manganite (γ -MnOOH) in dilute oxalate solution. Environ. Sci. Technol. 22, 62–70.
- Lind, C.J., Hem, J.D., 1993. Manganese minerals and associated fine particulates in the streambed of Pinal Creek, Arizona, U.S.A.: A mining-related acid drainage problem. Appl. Geochem. 8, 67–80.
- Liu, J., Aruguete, D.M., Murayama, M., Hochella, M.F., 2009. Influence of size and aggregation on the reactivity of an environmentally and industrially relevant nanomaterial. PbS) 43, 8178–8183.

- Luo, Y., Tan, W., Suib, S.L., Qiu, G., Liu, F., 2018. Dissolution and phase transformation processes of hausmannite in acidic aqueous systems under anoxic conditions. Chem. Geol. 487, 54–62.
- Manning, B.A., Fendorf, S.E., Bostick, B., 2002. Arsenic(III) oxidation and arsenic(V) adsorption reactions on synthetic birnessite. Environ. Sci. Technol. 36, 976–981.
- Mock, R.P., Schaefer, M.V., Pacheco, J.L., Lake, L., Lee, I., Ying, S.C., 2019. Influence of Fe(II) on arsenic(III) oxidation by birnessite in diffusion-limited systems. ACS Earth Sp. Chem. 3, 550–561.
- Nesbitt, H.W., Canning, G.W., Bancroft, G.M., 1998. XPS study of reductive dissolution of 7Å-birnessite by H₃AsO₃, with constraints on reaction mechanism. Geochem. Cosmochim. Acta 62, 2097–2110.
- Nicholson, K., Eley, M., 2007. Geochemistry of manganese oxides: metal adsorption in freshwater and marine environments. Geol. Soc. London, Spec. Publ. 119, 309–326.
- NIST X-ray Photoelectron Spectroscopy Database, 2000. NIST Standard Reference Database Number 20, n.D. National Institute of Standards and Technology, Gaithersburg MD, p. 20899.
- Ouvrard, S., de Donato, P., Simonnot, M.O., Begin, S., Ghanbaja, J., Alnot, M., Duval, Y. B., Lhote, F., Barres, O., Sardin, M., 2005. Natural manganese oxide: Combined analytical approach for solid characterization and arsenic retention. Geochem. Cosmochim. Acta 69, 2715–2724.
- Parikh, S.J., Lafferty, B.J., Meade, T.G., Sparks, D.L., 2010. Evaluating environmental influences on As^{III} oxidation kinetics by a poorly crystalline Mn-oxide. Environ. Sci. Technol. 44, 3772–3778.
- Parikh, S.J., Lafferty, B.J., Sparks, D.L., 2008. An ATR-FTIR spectroscopic approach for measuring rapid kinetics at the mineral/water interface. J. Colloid Interface Sci. 320, 177–185
- Peacock, C.L., 2009. Physiochemical controls on the crystal-chemistry of Ni in birnessite: Genetic implications for ferromanganese precipitates. Geochem. Cosmochim. Acta 73, 3568–3578.
- Peña, J., Duckworth, O.W., Bargar, J.R., Sposito, G., 2007. Dissolution of hausmannite (Mn_3O_4) in the presence of the trihydroxamate siderophore desferrioxamine B. Geochem. Cosmochim. Acta 71, 5661–5671.
- Post, J.E., 1999. Manganese oxide minerals: Crystal structures and economic and environmental significance. Proc. Natl. Acad. Sci. Unit. States Am. 96, 3447–3454.
- Post, J.E., 1992. Crystal Structures of Manganese Oxide Minerals. In: Skinner, H.C.W., Fitzpatrick, R.W. (Eds.), Biomineralization: Processes of Iron and Manganese: Modern and Ancient Environments. Catane Verlag, Cremlingen-Destedt, pp. 51–73.
- Ramstedt, M., Andersson, B.M., Shchukarev, A., Sjöberg, S., 2004. Surface properties of hydrous manganite (γ-MnOOH). A potentiometric, electroacoustic, and X-ray photoelectror spectroscopy study. Langmuir 20, 8224–8229.
- Ramstedt, M., Sjöberg, S., 2005. Phase transformations and proton promoted dissolution of hydrous manganite (γ -MnOOH). Aquat. Geochem. 11, 413–431.
- Ravel, B., Newville, M., 2005. ATHENA, artemis, hephaestus: Data analysis for X-ray absorption spectroscopy using IFEFFIT. J. Synchrotron Radiat. 12, 537–541.
- Scott, M.J., Morgan, J.J., 1995. Reactions at oxide surfaces. 1. Oxidation of As(III) by synthetic birnessite. Environ. Sci. Technol. 29, 1898–1905.
- Shaughnessy, D.A., Nitsche, H., Booth, C.H., Shuh, D.K., Waychunas, G.A., Wilson, R.E., Gill, H., Cantrell, K.J., Serne, R.J., 2003. Molecular interfacial reactions between Pu (VI) and manganese oxide minerals manganite and hausmannite. Environ. Sci. Technol. 37, 3367–3374.
- Shumlas, S.L., Singireddy, S., Thenuwara, A.C., Attanayake, N.H., Reeder, R.J., Strongin, D.R., 2016. Oxidation of arsenite to arsenate on birnessite in the presence of light. Geochem. Trans. 17, 1–10.
- Silva, G.C., Almeida, F.S., Dantas, M.S.S., Ferreira, A.M., Ciminelli, V.S.T., 2013. Raman and IR spectroscopic investigation of As adsorbed on Mn_3O_4 magnetic composites. Spectrochim. Acta Part A Mol. Biomol. Spectrosc. 100, 161–165.
- Simanova, A.A., Kwon, K.D., Bone, S.E., Bargar, J.R., Refson, K., Sposito, G., Peña, J., 2015. Probing the sorption reactivity of the edge surfaces in birnessite nanoparticles using nickel(II). Geochem. Cosmochim. Acta 164, 191–204.
- Simanova, A.A., Pena, J., 2015. Time-resolved investigation of cobalt oxidation by Mn (III)-rich δ -MnO₂ using quick X-ray absorption spectroscopy. Environ. Sci. Technol. 49, 10867–10876.
- Smedley, P.L., Kinniburgh, D.G., 2002. A review of the source, behaviour and distribution of arsenic in natural waters. Appl. Geochem. 17, 517–568.
- Smith, P.G., Koch, I., Gordon, R.A., Mandoli, D.F., Chapman, B.D., Reimer, K.J., 2005. X-ray absorption near-edge structure analysis of arsenic species for application to biological environmental simples. Environ. Sci. Technol. 39, 248–254.
- Song, B., Cerkez, E.B., Elzinga, E.J., Kim, B., 2020. Effects of Ni incorporation on the reactivity and stability of hausmannite (Mn₃O₄): Environmental implications for Mn, Ni, and As solubility and cycling. Chem. Geol. 558, 119862.
- Song, R., Wang, H.-J., Shou-Hua, F., 2012. Solvothermal preparation of Mn_3O_4 nanoparticles and effect of temperature on particle size. Chem. Res. Chin. Univ. 28, 577–580.
- Taujale, S., Baratta, L.R., Huang, J., Zhang, H., 2016. Interactions in ternary mixtures of MnO₂, Al₂O₃, and natural organic matter (NOM) and the impact on MnO₂ oxidative reactivity. Environ. Sci. Technol. 50, 2345–2353.
- Taujale, S., Zhang, H., 2012. Impact of interactions between metal oxides to oxidative reactivity of manganese dioxide. Environ. Sci. Technol. 46, 2764–2771.
- Taylor, R.M., McKenzie, R.M., 1966. The association of trace elements with manganese minerals in Australian soils. Soil Res. 4, 29–39.
- Tournassat, C., Charlet, L., Bosbach, D., Manceau, A., 2002. Arsenic(III) oxidation by birnessite and precipitation of manganese(II) arsenate. Environ. Sci. Technol. 36, 493–500.
- Villalobos, M., 2015. The role of surface edge sites in metal(loid) sorption to poorlycrystalline birnessites. ACS Symp. Ser. 1197, 65–87.

- Weaver, R.M., Hochella, M.F., 2003. The reactivity of seven Mn-oxides with Cr³⁺_(aq): A comparative analysis of a complex, aqueous environmentally important redox reaction. Am. Mineral. 88, 2016–2027.
- Weaver, R.M., Hochella, M.F., Ilton, E.S., 2002. Dynamic processes occurring at the CrIIIaq-manganite (y-MnOOH) interface: Simultaneous adsorption, microprecipitation, oxidation/reduction, and dissolution. Geochem. Cosmochim. Acta 66, 4119–4132.
- Wilk, P.A., Shaughnessy, D.A., Wilson, R.E., Nitsche, H., 2005. Interfacial interactions between Np(V) and manganese oxide minerals manganite and hausmannite. Environ. Sci. Technol. 39, 2608–2615.
- Wu, Y., Kukkadapu, R.K., Livi, K.J.T., Xu, W., Li, W., Sparks, D.L., 2018. Iron and arsenic speciation during As(III) oxidation by manganese oxides in the presence of Fe(II): Molecular-level characterization using XAFS, Mössbauer, and TEM analysis. ACS Earth Sp. Chem. 2, 256–268.
- Yin, H., Feng, X., Qiu, G., Tan, W., Liu, F., 2011. Characterization of Co-doped birnessites and application for removal of lead and arsenite. J. Hazard Mater. 188, 341–349.

- Yin, H., Li, H., Wang, Y., Ginder-Vogel, M., Qiu, G., Feng, X., Zheng, L., Liu, F., 2014. Effects of Co and Ni co-doping on the structure and reactivity of hexagonal birnessite. Chem. Geol. 381, 10–20.
- Ying, S.C., Kocar, B.D., Fendorf, S., 2012. Oxidation and competitive retention of arsenic between iron- and manganese oxides. Geochem. Cosmochim. Acta 96, 294–303.
- Zhang, G., Liu, F., Liu, H., Qu, J., Liu, R., 2014. Respective role of Fe and Mn oxide contents for arsenic sorption in iron and manganese binary oxide: An X-ray absorption spectroscopy investigation. Environ. Sci. Technol. 48, 10316–10322.
- Zhang, G.S., Qu, J.H., Liu, H.J., Liu, R.P., Li, G.T., 2007. Removal mechanism of As(III) by a novel Fe-Mn binary oxide adsorbent: Oxidation and sorption. Environ. Sci. Technol. 41, 4613–4619.
- Zhang, H., Taujale, S., Huang, J., Lee, G.J., 2015. Effects of NOM on oxidative reactivity of manganese dioxide in binary oxide mixtures with goethite or hematite. Langmuir 31, 2790-2799.
- Zhou, J., Zhou, X., Yang, K., Cao, Z., Wang, Z., Zhou, C., Baig, S.A., Xu, X., 2020. Adsorption behavior and mechanism of arsenic on mesoporous silica modified by iron-manganese binary oxide (FeMnO_x/SBA-15) from aqueous systems. J. Hazard Mater. 384, 121229.